ELSEVIER

Journal of Organometallic Chemistry 484 (1994) 209–224

Journal of Organometallic Chemistry

Synthesis, structural characterization and photophysical properties of ethyne–gold(I) complexes

Thomas E. Müller [a], Sam Wing-Kin Choi [b], D. Michael P. Mingos [a,*], Don Murphy [a], David J. Williams [a], Vivian Wing-Wah Yam [b]

[a] *Department of Chemistry, Imperial College of Science, Technology and Medicine, South Kensington, London SW7 2AY, UK*
[b] *Department of Chemistry, University of Hong Kong, Pokfulam Road, Hong Kong, Hong Kong*

Received 6 April 1994

Abstract

A series of closely related ethynyl–gold(I) complexes was synthesized by reaction of $Au(PR_3)Cl$ with an alkaline solution of the ethyne. The molecular structures of the ethynediyl–digold complexes $NpPh_2P–Au–C{\equiv}C–Au–PNpPh_2 \cdot 2CHCl_3$ (**1**) (Np = naphthyl), $Np_2PhP–Au–C{\equiv}C–Au–PNp_2Ph \cdot 6CHCl_3$ (**2**) and $Fc_2PhP–Au–C{\equiv}C–Au–PFc_2Ph \cdot 4EtOH$ (**3**) (Fc = ferrocenyl) and the phenylethynyl–gold complex $Fc_2PhP–Au–C{\equiv}C–Ph$ (**4**) were determined by single-crystal X-ray diffraction measurements. Variation of the phosphines does not have a significant influence on the bonding in the central P–Au–C≡C unit, the Au–P and Au–C distances being in the ranges 2.274(4)–2.289(5) and 1.983(8)–2.002(6) Å, respectively. Although none of the compounds have short Au · · · Au contacts, compounds **1** and **2** do show novel C–H · · · π interactions between the proton of $CHCl_3$ and the π-electron system of the C≡C bond. In **1**, pairs of $CHCl_3$ molecules are located with their protons 2.4 Å from the centre of the C≡C bond with the C–H bond directed orthogonally towards the centre of the ethyne bond. In **2**, two pairs of $CHCl_3$ molecules are located around the C≡C bond, with 2.5 Å between the proton and the centre of the triple bond, resulting in a pseudo-octahedral arrangement around C≡C. In addition to the C–H · · · π interactions, the structures of **1** and **2** also show a range of intermolecular aromatic–aromatic interactions. The first structural determination of naphthylphosphines resulted in estimates of their steric requirements. The UV–visible spectra of CH_2Cl_2 solutions of the ethynediyl compounds exhibit intense absorption bands at ca. 300 nm assignable to intraligand transitions. Excitation of solid sample or fluid solution of complex **1** at $\lambda > 330$ nm resulted in intense long-lived luminescence. Excitation of a solution of **2** at 350 and 380 nm led to different types of photoluminescence.

Keywords: Gold; Alkyne; UV–visible spectra; X-ray structure C–H · · · π interactions; Phosphine

1. Introduction

In striking contrast to the wide and selective applications of organo- and alkynyl–copper(I) complexes in organic chemistry, the use of the heavier gold congener has not been extensively studied. Few examples of σ-ethynyl derivatives of gold have been reported although they are among the thermally most stable organogold(I) compounds. Donor ligands such as tertiary phosphines, amines, phosphites and electrophiles can rapidly cleave the gold–carbon bond, making these complexes ideal starting materials for gold(I) chemistry.

Some examples of gold complexes involving phenylethyne have been synthesized and structurally characterized. The related bisaurated ethynes have been less studied because of their low solubilities. Only the two isomorphous ethynediyl compounds $R_3P–Au–C{\equiv}C–Au–PR_3 \cdot nC_6H_6$ ($PR_3 = PPh_3 (n = 2)$ and $P(m\text{-}Tol)_3$ ($n = 0$ and 1)) have been structurally characterized [1].

We report here the synthesis of further examples of (μ-ethyne)bis(phosphine–gold(I)) complexes involving naphthyldiphenylphosphine, dinaphthylphenylphos-

* Corresponding author.

SSDI 0022-328X(94)24734-Z

phine, trinaphthylphosphine and diferocenylphenylphosphine. The structural characterizations of the compounds $NpPh_2P-Au-C\equiv C-Au-PNpPh_2 \cdot 2CHCl_3$ (**1**) (Np = naphthyl), $Np_2PhP-Au-C\equiv C-Au-PNp_2Ph \cdot 6CHCl_3$ (**2**) and $Fc_2PhP-Au-C\equiv C-Au-PFc_2Ph \cdot 4EtOH$ (**3**) (Fc = ferrocenyl) are reported together with the synthesis and structural characterization of $Fc_2PhP-Au-C\equiv C-Ph$ (**4**). For purposes of comparison phenylethynephosphine–gold(I) complexes were prepared from $[Au-C\equiv C-Ph]_x$ with triphenylphosphine and methyldiphenylphosphine. By slight modification of the procedure for the preparation of **1–3**, the synthesis could be directed towards the monoaurated ethynyl complexes $R_3P-Au-C\equiv CH$. For naphthyldiphenylphosphine and biphenyldiphenylphosphine the product was isolated and characterized.

Interestingly, although hundreds of structures of triphenylphosphine complexes have been reported, none of the corresponding naphthyl complexes have been studied. This series of compounds thus affords the opportunity of studying the steric requirements of naphthylphosphine ligands and of investigating the effect of intermolecular interactions between the aromatic rings. Several chemists have suggested that attractive [2] intermolecular arene–arene graphitic-like interactions [3] in coordination and cluster compounds are important [4], but to date no attempt has been made to enhance these effects by using polyaromatic substituents.

The luminescent photophysical behaviour exhibited by this series of novel coordinatively unsaturated ethyne–gold(I) complexes was of interest in view of recent studies on the photophysics and photochemistry of luminescent d^{10} metal phosphine and alkynyl metal systems [5]. These complexes are of particular interest because of the presence of coordinatively unsaturated metal centres and the fact that their lowest electronic excited states are usually long-lived and powerful reductants.

2. Results and discussion

2.1. Synthesis

The ethynylgold complexes $R_3P-Au-C\equiv C-Au-PR_3$ were prepared by modifications of the synthesis reported by Cross and Davidson [6]. In this method, sodium ethoxide is added to a suspension of $[Au(PR_3)Cl]$ in ethanol, and the mixture is then treated with the ethyne. The product is normally sparingly soluble in ethanol and can be obtained essentially pure by filtration. This method also gives good yields for phenylethynyl–gold(I) complexes and $Fc_2PhP-Au-C\equiv C-Ph$ was obtained in excellent yields (96%) by this route. For purposes of comparison the complexes $Ph_3P-Au-C\equiv C-Ph$ (**5**) and $MePh_2P-Au-C\equiv C-Ph$ (**6**) were prepared by reacting $[Au-C\equiv C-Ph]_x$ with the corresponding phosphine [7].

The synthesis of the ethynediyl–digold complexes has some interesting subtleties. If phosphines such as PNp_xPh_{3-x} and $PBpPh_2$ (Bp = biphenyl) are used, the reaction starting from $[Au(PR_3)Cl]$ results in a mixture of mono- and di-aurated ethyne complexes, $R_3P-Au-C\equiv CH$ and $R_3P-Au-C\equiv C-Au-PR_3$. At times these compounds are difficult to separate because of their very low solubilities in organic solvents. To increase the reactivity of the $[Au(PR_3)Cl]$, it was dissolved in a small volume of THF and the filtered solution was run into ethanol. This resulted in a very reactive colloidal suspension. After the solution was made alkaline with KO^tBu in ethanol, ethyne was bubbled through the solution. After a short period, 1–30 min depending on the phosphine, an intense white precipitate separated, and proved to be $R_3P-Au-C\equiv C-Au-PR_3$. Prolonged reaction times led to an increasingly higher proportion of the monoaurated ethyne $R_3P-Au-C\equiv CH$ in the product mixture. By optimization of the conditions the reaction could be directed towards the formation of either product. Good to excellent yields of the products were obtained. The compounds **1**, **2**, $[Np_3P-Au-C\equiv C-Au-PNp_3]$ (**7**), $[Ph_3P-Au-C\equiv C-Au-PPh_3]$ (**8**), $[NpPh_2P-Au-C\equiv CH]$ (**9**) and $[BpPh_2P-Au-C\equiv CH]$ (**10**) were isolated and characterized using this approach.

IR spectroscopy proved to be very valuable for monitoring the reaction. During the synthesis of **1**, **2**, **8–10**, IR spectra of the reaction mixture were taken. The Au–Cl peak at ca. 330 cm^{-1} decreased in intensity during the course of the reaction and disappeared when the precipitate formed. No $\nu(C\equiv C)$ stretch of the ethynediyl compounds was observed in the IR spectrum because of the centrosymmetric nature of the compounds, but a very strong peak was observed in the Raman spectrum between 2002 and 2012 cm^{-1}. As the reaction with ethyne proceeded an increasingly intense peak at ca. 2000 cm^{-1} appeared in the IR spectrum owing to the formation of monosubstituted compounds with the IR-active $C\equiv CH$ group.

An interesting feature of **1** and **2** is their solubility. When these compounds are synthesized and separated from the ethanol solution they are fairly soluble in CH_2Cl_2 and $CHCl_3$. However, after recrystallization it is nearly impossible to redissolve them in the same solvent. For further experiments the compounds were therefore not recrystallized, but stirred with MeOH/H_2O (1:1) overnight to remove all impurities and used as obtained after drying.

$Fc_2PhPAuCl$ behaves differently. Following the procedure mentioned above, no sign of the formation of a monoaurated species could be detected even after very long reaction times (2 days). The solubility of the

product (3) is considerably higher in organic solvents, probably owing to a lower extent of intermolecular interactions in the solid state.

2.2. Molecular structure of $NpPh_2P$–Au–C≡C–Au–$PNpPh_2 \cdot 2CHCl_3$ (1)

A perspective view of the complex, which has a crystallographic centre of symmetry at the centre of the ethyne bond, is shown in Fig. 1. The central C≡C bond has a length of 1.222(16) Å, the Au–C bond 1.983(8) Å and the Au–P bond 2.277(2) Å (see Table 1). These agree well with the values for Ph_3P–Au–C≡C–Au–$PPh_3 \cdot 2C_6H_6$ (1.13(2), 2.02(1) and 2.270(4) Å, respectively), (*m*-Tol)$_3$P–Au–C≡C–Au–P(*m*-Tol)$_3$ (1.19(2), 2.002(9) and 2.284(3) Å, respectively) and (*m*-Tol)$_3$P–Au–C≡C–Au–P(*m*-Tol)$_3 \cdot C_6H_6$ (1.19(2), 2.00(1) and 2.280(3) Å, respectively). The P–C bonds range in length from 1.811(9) to 1.819(8) Å and the Au–P–C angle is 111.7(3)° for the naphthyl substituent and 114.7(3)° and 113.8(3)° for the phenyl groups. The P–Au–C≡C unit deviates slightly from linearity, with an angle at C(1) of 174(1)° and at Au(1) of 175.8(2)°. The Au–C≡C–Au chain adopts an *anti* geometry (Au(1)–C(1)–C(1′)–Au(1′) torsion angle = 180°).

In contrast to many gold(I) compounds which frequently exhibit short Au–Au intermolecular contacts, the gold atom in 1 is linearly coordinated with no close approaches to the metal centres. The nearest intramolecular non-bonded contact is to the naphthyl hydrogen H(18) at 2.92 Å and the nearest intermolecular contact is again to a naphthyl proton (2.93 Å to H(15)).

An analysis of the packing of the molecules reveals significant aromatic–aromatic, face-to-face and edge-to-face interactions. Pairs of centrosymmetrically related naphthalene rings are aligned parallel and overlapping (Fig. 2) with a mean interplanar separation of 3.59 Å. There are, in addition, edge-to-face interactions between the phenyl ring A (C(21)–C(26)) and phenyl ring B (C(31)–C(36)) of an adjacent glide related molecule. The ring centroid–centroid distance between A and B is 5.3 Å with the *p*-proton H(24) lying 2.6 Å from the mean plane of ring B. The centroid–centroid vector is inclined at an angle of 80° to the mean plane of ring B. This interaction extents through the crystal in the 101 direction.

The solvent $CHCl_3$ molecules are located in constricted channels which extend along the crystallographic *b* direction (Fig. 3). No interaction of chloroform with the gold atoms could be detected; the closest contact is between Cl(3) and Au(1) with a distance of 4.21 Å. However, centrosymmetrically related pairs of chloroform molecules are positioned with their C–H bonds directed orthogonally towards the centre of the ethyne C(1)–C(1′) bond (Fig. 4).

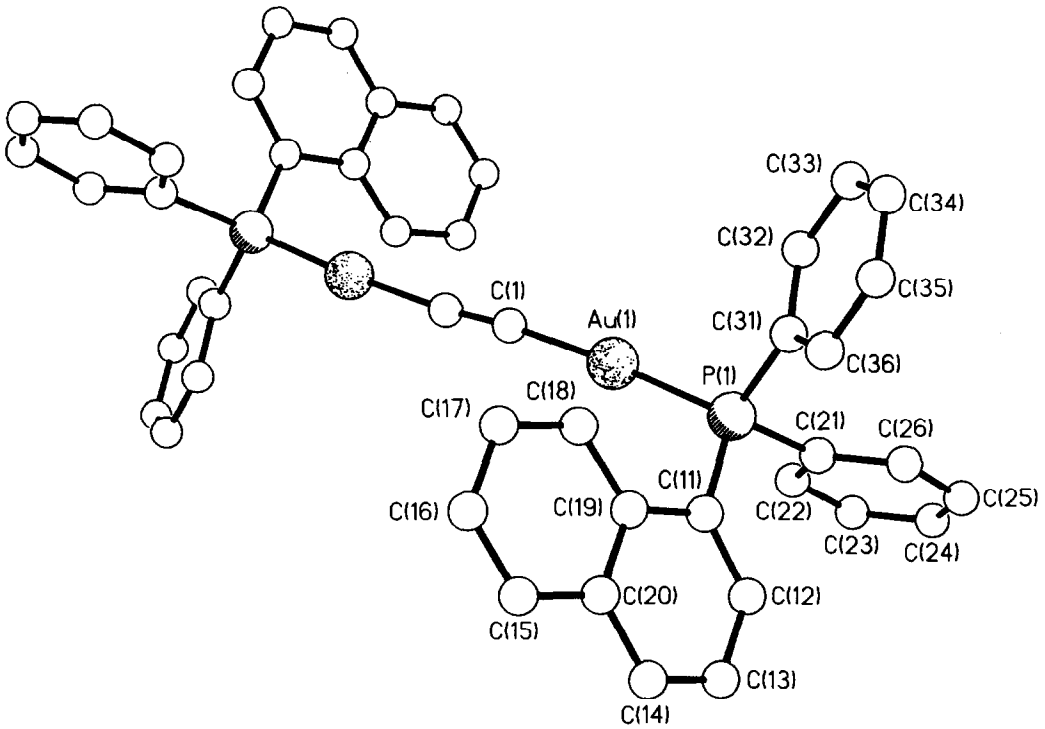

Fig. 1. Molecular structure of $NpPh_2P$–Au–C≡C–Au–$PNpPh_2$ (1), showing the atomic labelling scheme.

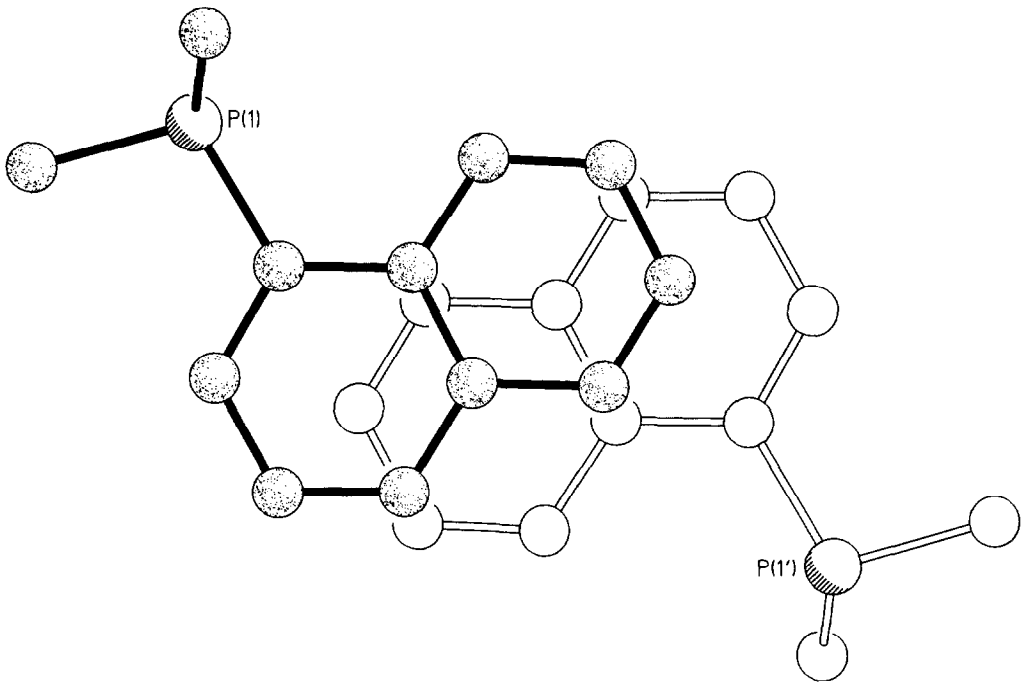

Fig. 2. Aromatic–aromatic stacking interaction of centrosymmetrically related naphthyl groups in **1**.

The perpendicular distance of H(41) to the triple bond is 2.41 Å and its distance to the bond centre is 2.42 Å. The H(41)–bond centre–H(41′) vector is inclined by 85° to the triple bond and the C–H–centroid angle is 174.3°. This arrangement is clearly indicative of pairs of C–H $\cdots$ π interactions [8], which are favoured both by the acidic nature of the $CHCl_3$ protons and by the donation of electrons by the gold atoms into the triple bond. Similar interactions have been observed involving O–H $\cdots$ π arrangements [9].

2.3. Molecular structure of Np_2PhP–Au–C≡C–Au–$PNp_2Ph \cdot 6CHCl_3$ (2)

Fig. 5 shows a perspective view of **2** together with the atom numbering used. Complex **2** also has a crystallographic symmetry centre, which is located in the middle of the C≡C bond. Bond lengths for the P–Au–C≡C–Au–P chain are 1.225(34) Å for C≡C, 1.986(17) Å for Au–C and 2.289(5) Å for Au–P; these are comparable with those in **1** (see Table 2). The P–C bond lengths do not differ significantly and range from 1.811(20) to 1.817(12) Å. The Au–P–C angles range from 107.5(6)° for the phenyl ring to 113.2(5)° and 118.5(7)° for the naphthyl rings.

Table 1
Selected bond lengths (Å) and angles (°) for **1**

Au(1)–P(1)	2.277(2)	P(1)–C(21)	1.811(7)
Au(1)–C(1)	1.983(8)	P(1)–C(31)	1.811(9)
P(1)–C(11)	1.819(8)	C(1)–C(1A)	1.222(16)
P(1)–Au(1)–C(1)	175.8(2)	Au(1)–C(1)–C(1A)	174.2(10)
Au(1)–P(1)–C(11)	111.7(3)	P(1)–C(11)–C(12)	119.7(6)
Au(1)–P(1)–C(21)	114.7(3)	P(1)–C(11)–C(19)	121.0(6)
C(11)–P(1)–C(21)	105.1(4)	P(1)–C(21)–C(22)	117.5(7)
Au(1)–P(1)–C(31)	113.8(3)	P(1)–C(21)–C(26)	122.7(7)
C(11)–P(1)–C(31)	106.5(4)	P(1)–C(31)–C(32)	117.5(7)
C(21)–P(1)–C(31)	104.2(4)	P(1)–C(31)–C(36)	122.5(7)

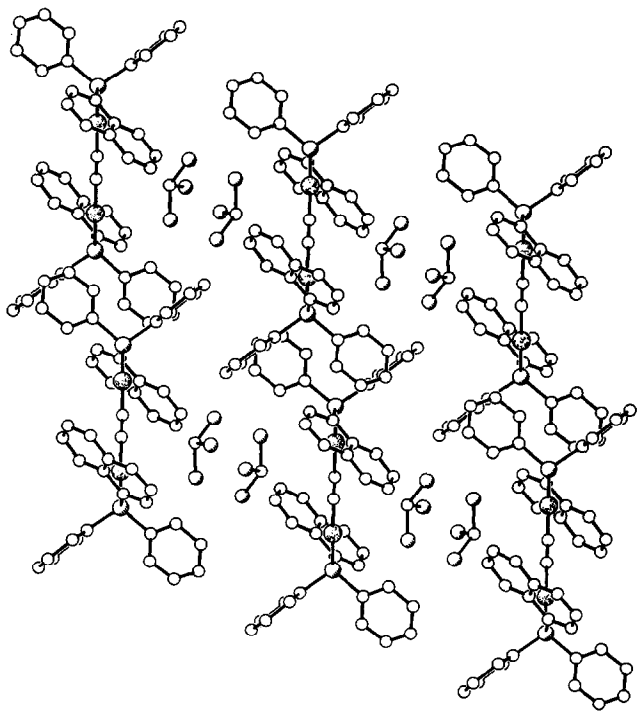

Fig. 3. Packing of the molecules in **1**, viewed down the *b*-axis, in parallel projection.

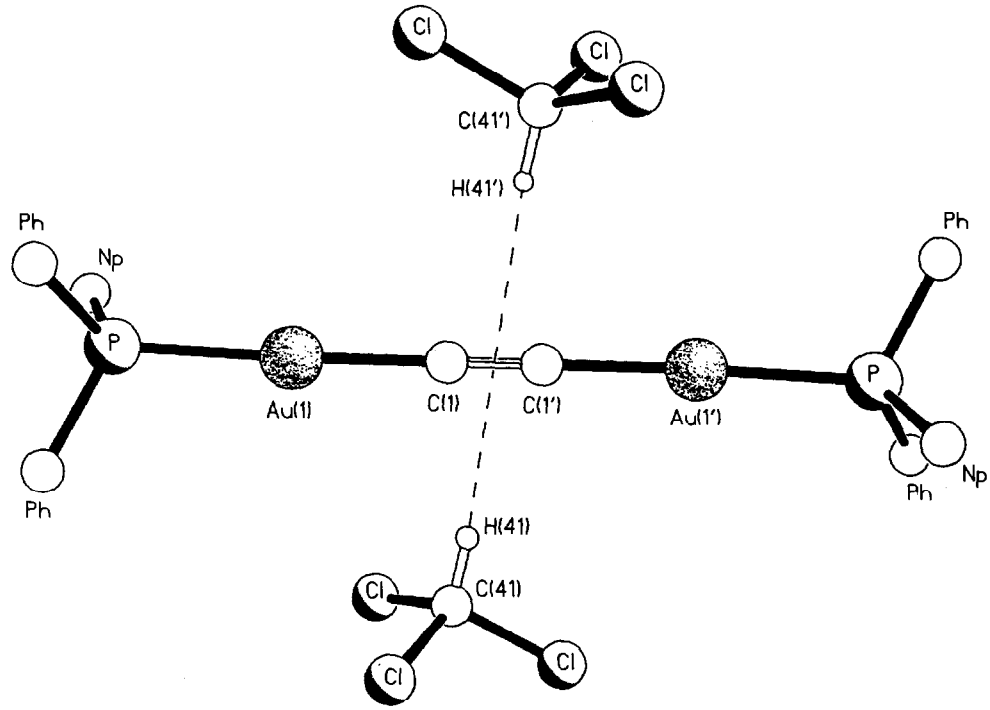

Fig. 4. C–H · · · π interactions in **1**.

The P–Au–C≡C angle is close to linear (178(2)° at C(1) and 176.6(6)° at Au(1)) and the torsion angle for Au(1)–C(1)–C(1a)–Au(1a) is, as consequence of the crystallographic symmetry, 180°. As in structure **1** there are no close approaches to the gold centres, the closest intramolecular contact being 2.89 Å to the phenyl hydrogen H(32) and the closest intermolecular contact being 3.32 Å to one of the naphthyl protons, H(14).

The structure, which is heavily solvated with $CHCl_3$ molecules, consists of domains populated alternately by

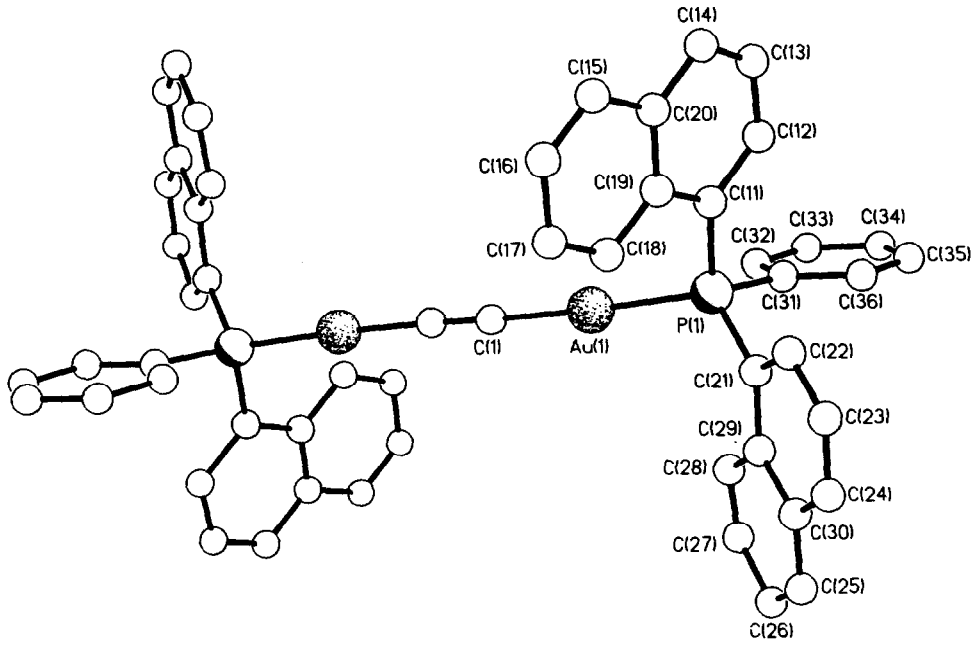

Fig. 5. Molecular structure of Np_2PhP–Au–C≡C–Au–PNp_2Ph (**2**), showing the atomic labelling scheme.

Table 2
Selected bond lengths (Å) and angles (°) for **2**

Au(1)–P(1)	2.289(5)	P(1)–C(21)	1.817(12)
Au(1)–C(1)	1.986(17)	P(1)–C(31)	1.811(20)
P(1)–C(11)	1.813(18)	C(1)–C(1A)	1.225(34)
P(1)–Au(1)–C(1)	176.6(6)	Au(1)–C(1)–C(1A)	177.8(23)
Au(1)–P(1)–C(11)	107.5(6)	P(1)–C(11)–C(12)	117.2(14)
Au(1)–P(1)–C(21)	118.5(7)	P(1)–C(11)–C(19)	123.2(16)
C(11)–P(1)–C(21)	106.7(6)	P(1)–C(21)–C(22)	119.7(13)
Au(1)–P(1)–C(31)	113.2(5)	P(1)–C(21)–C(29)	121.2(9)
C(11)–P(1)–C(31)	106.3(10)	P(1)–C(31)–C(32)	118.3(14)
C(21)–P(1)–C(31)	104.0(7)	P(1)–C(31)–C(36)	121.8(11)

the solvent molecules and the Au–C≡C–Au linkages or by the aromatic components (Fig. 6). These layers extend in the crystallographic *b* and *c* directions.

Aromatic interactions again play a dominant role in the packing of the molecules of **2** in the crystal. Within the aromatic domains there are parallel naphthyl–naphthyl stacking interactions between centrosymmetrically related rings. These occur with differing degrees of ring overlap for both the C(11)–C(20) ring (ring–ring separation 3.46 Å) and for the C(21)–C(30) ring (ring–ring separation 3.53 Å). There are additional edge-to-face interactions between one naphthyl group (C(21)–C(30)) and an adjacent phenyl group (C(31')–C(36')). The two ring systems are aligned essentially perpendicular with an angle between their mean planes of 87.4°. The edge of the phenyl group is directed towards the centre of the naphthyl group with a distance between the phenyl ring proton H(34) and the mean plane of the naphthyl system of 2.73 Å. The distances between the centroid of the phenyl group to the centroids of the two rings of the naphthyl system are 5.14 and 5.15 Å.

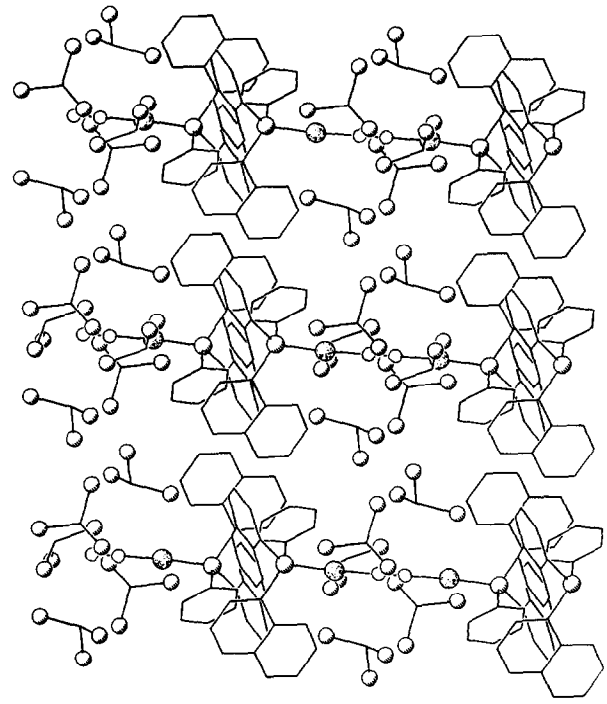

Fig. 6. *c*-Axis projection of the packing of the molecules in **2**.

The solvent domains are only partially intersected by the Au–C≡C–Au linkages. This results in fairly open channels which permit the solvent to diffuse out

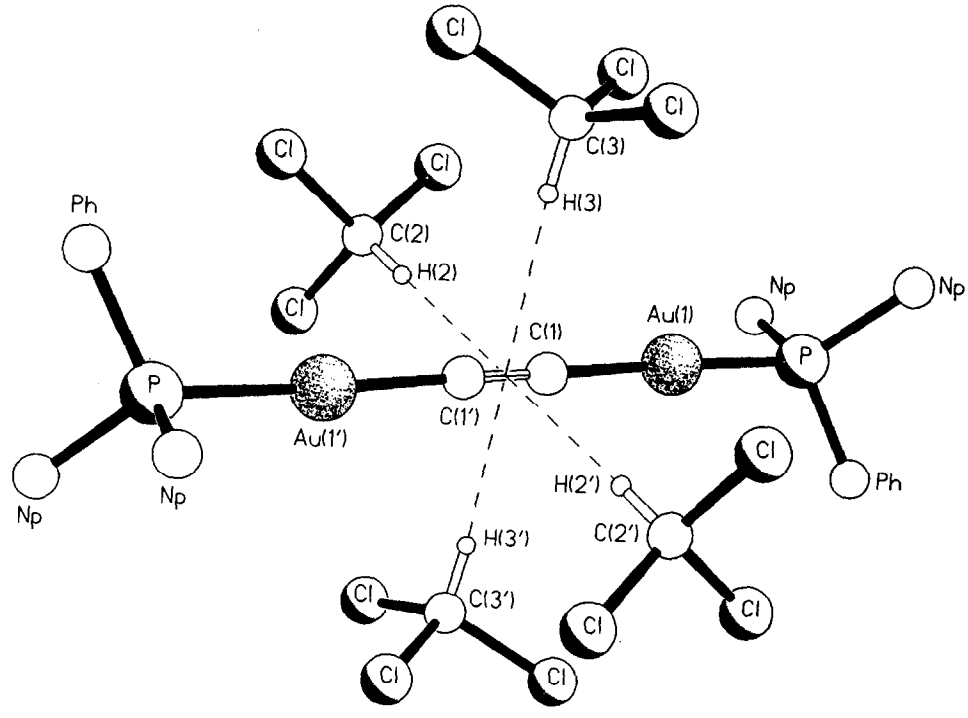

Fig. 7. Pseudo-octahedral arrangement of $CHCl_3$ around the C(1)–C(1) ethyne bond in **2**, showing the C–H · · · π interactions.

of the lattice. An inspection of the solvent region of the lattice reveals pairs of $CHCl_3$ molecules oriented with their C–H bond directed towards the centre of the ethyne C(1)≡C(1′) bond. The arrangement is directly analogous to that observed in **1** except that in **2** there are two pairs of $CHCl_3$ molecules each arranged with their CH · · · π · · · HC axis oriented approximately orthogonally (Fig. 7). The distances of H(2) and H(3) to the centre of the ethyne bond are 2.58 and 2.50 Å respectively. The H(2)–H(2′) and H(3)–H(3′) vectors are inclined by 84.8° and 89.1° to the C(1)≡C(1′) bond and by 89.1° to each other thus forming a pseudo-octahedral type arrangement. The associated C–H–centroid angles are 166.6° at H(2) and 172.7° at H(3). Although the C–H–centroid distances are slightly longer than those observed in **1** we still believe they constitute significant C–H · · · π interactions. As previously, these interactions are favoured by the acidity of the C–H bond in $CHCl_3$ and by the back-donation of electron density from the gold into the C≡C bond. The third pair of $CHCl_3$ molecules is not involved in any significant intermolecular interactions.

Table 3
Selected bond lengths (Å) and angles (°) for **3**

Au(1)–P(1)	2.276(2)	Fe(2)–C(22)	2.028(9)
Au(1)–C(1)	2.002(6)	Fe(2)–C(23)	2.041(7)
Fe(1)–C(11)	2.032(7)	Fe(2)–C(24)	2.053(6)
Fe(1)–C(12)	1.996(6)	Fe(2)–C(25)	2.037(6)
Fe(1)–C(13)	2.043(7)	Fe(2)–C(26)	2.026(7)
Fe(1)–C(14)	2.050(6)	Fe(2)–C(27)	2.027(8)
Fe(1)–C(15)	2.040(7)	Fe(2)–C(28)	1.998(11)
Fe(1)–C(16)	2.039(6)	Fe(2)–C(29)	2.010(13)
Fe(1)–C(17)	2.005(9)	Fe(2)–C(30)	2.018(10)
Fe(1)–C(18)	2.013(12)	P(1)–C(11)	1.789(7)
Fe(1)–C(19)	2.027(9)	P(1)–C(21)	1.786(7)
Fe(1)–C(20)	2.050(8)	P(1)–C(31)	1.817(6)
Fe(2)–C(21)	2.035(7)	C(1)–C(1A)	1.196(12)
P(1)–Au(1)–C(1)	175.9(2)	Fe(1)–C(11)–P(1)	127.5(3)
Au(1)–P(1)–C(11)	116.0(2)	P(1)–C(11)–C(12)	127.2(4)
Au(1)–P(1)–C(21)	112.0(2)	P(1)–C(11)–C(15)	126.5(6)
C(11)–P(1)–C(21)	103.3(3)	Fe(2)–C(21)–P(1)	127.2(3)
Au(1)–P(1)–C(31)	117.5(2)	P(1)–C(21)–C(22)	125.2(6)
C(11)–P(1)–C(31)	102.3(3)	P(1)–C(21)–C(25)	128.0(4)
C(21)–P(1)–C(31)	104.0(3)	P(1)–C(31)–C(32)	119.8(4)
Au(1)–C(1)–C(1A)	177.9(11)	P(1)–C(31)–C(36)	120.0(5)

2.4. *Molecular structure of Fc_2PhP–Au–C≡C–Au–$PFc_2Ph \cdot 4EtOH$ (3)*

The structure of **3**, like those of **1** and **2** is centrosymmetric with respect to the C≡C bond (Fig. 8). The C≡C, Au–C and Au–P bonds are 1.196(12), 2.002(6) and 2.276(2) Å and do not differ significantly from those observed in **1** and **2** (see Table 3). Similarly, the P–Au–C≡C unit is again basically linear, with an angle at C(1) of 178(1)° and at Au(1) of 175.9(2)°. The P–C bond distances range from 1.786(7) for one of the ferrocenyl-C to 1.817(6) for the phenyl-C. The Au–P–C angles are 116.0(2)° and 112.0(2)° for the ferrocenyl-C and 117.5(2)° for the phenyl-C atoms.

Each of the ferrocenyl moieties has an eclipsed geometry with only small in-plane rotations of the ring with respect to each other (6.4° for C(11) to C(20) and 9.7° for C(21) to C(30)). The cyclopentadienyl rings within of each ferrocenyl unit are not perfectly parallel, with mean interplanar angles of 2.4° and 3.6°, respectively. The two substituent ferrocenyl units are ori-

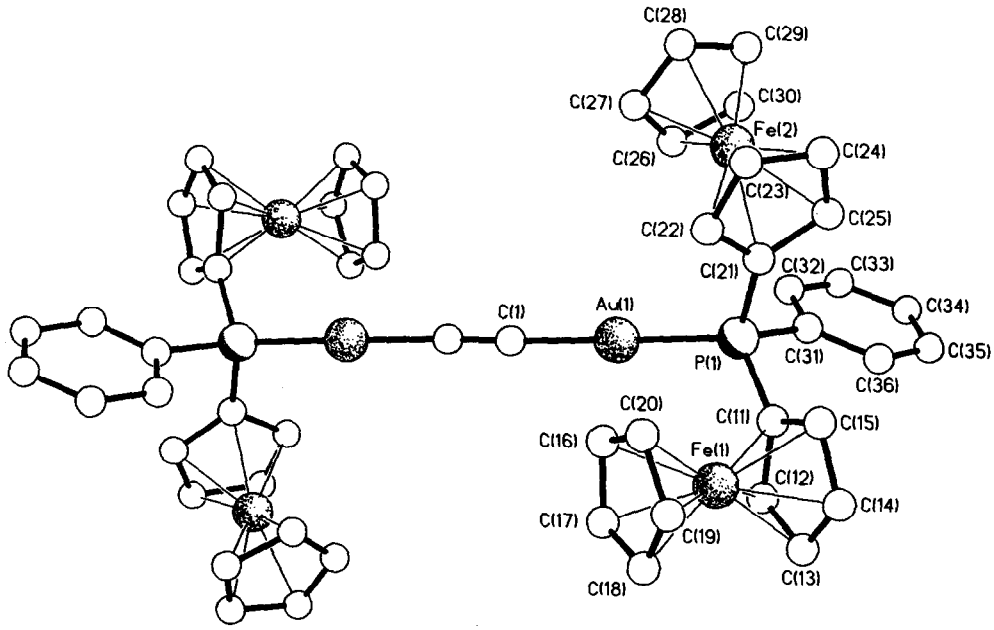

Fig. 8. Molecular structure of Fc_2PhP–Au–C≡C–Au–PPc_2Ph (**3**) showing the atomic labelling scheme.

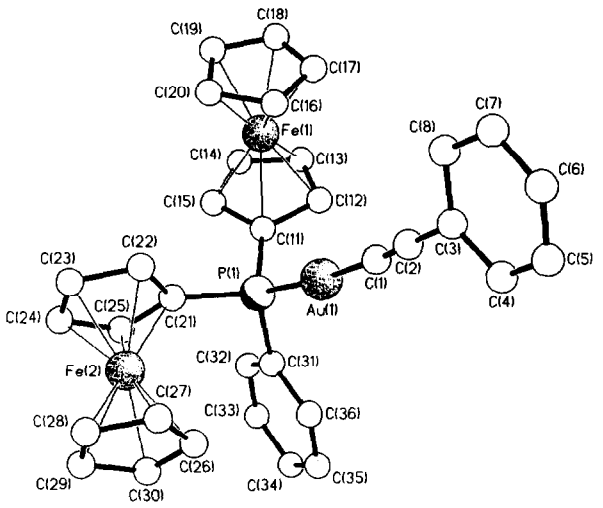

Fig. 9. Molecular structure of Fc_2PhP–Au–C≡C–Ph (1) showing the atomic labelling scheme.

ented essentially orthogonal with respect to each other with a dihedral angle of 88° between the mean planes of C(11)–C(15) and C(21)–C(25).

As in structures 1 and 2, there are no close approaches to the gold centres. However, pairs of partial weight ethanol molecules are oriented with their oxygen atoms positioned 3.10 Å from the centre of the ethyne bond. The O–O vector is inclined orthogonally to the C(1)–C(1′) bond. Although the positions of the OH hydrogen atoms could not be located, we believe, in the light of the observed C–H...π interactions in structures 1 and 2 that they are probably directed towards the ethyne π-system and represent O–H...π interactions. Analogous O–H···π interactions have been detected in the structure of *cis*-$[Me_2C(OH)C{\equiv}C]_2Pt(PPh_3)_2 \cdot H_2O$ [9,10]. There is a second partial occupancy ethanol molecule which lies at a hydrogen bonding distance from the first. The EtOH molecules are located in restricted channels which extend down the crystallographic *b* direction.

2.5. Molecular structure of Fc_2PhP–Au–C≡CPh (4)

The structure of complex 4 is shown in Fig. 9, together with the atomic labelling scheme. The intramolecular features are very similar to those of 3. The C≡C bond length, 1.172(21) Å, is at the short end of the range found for transition metal acetylides. The bond lengths for Au–C, 2.011(15) Å, Au–P, 2.274(4) Å, and C(2)–C(3), 1.478(22) Å, are normal (see Table 4). The ethynyl group deviates slightly from linearity with Au(1)–C(1)–C(2) being 177(1)°. The arrangement within the phosphine is very similar to that in 3. The planes of the C(11)–C(15) and C(21)–C(25) rings are approximately orthogonal (interplanar angle 76°). One of the ferrocenyl units (Fe(2)) adopts a near-eclipsed geometry for its C_5H_5 and C_5H_4 rings (ca. 5°). The arrangement for the Fe(1) based unit is closer to staggered, however, with a mean twist about the ring centroid–centroid vector of ca. 20°. As in 3, there are small departures from coplanarity of the rings within each ferrocenyl unit (3.1° for Fe(1) and 3.3° for Fe(2)).

Inspection of the packing of the molecules does not reveal any intermolecular interactions other than Van der Waals, the shortest intermolecular contact being 2.8 Å between C(2) and H(29).

2.6. Estimation of the steric requirement of the phosphines

Since structures of naphthylphosphine complexes have not previously been described, it was of interest to use the above structural data to compare the Tolman cone angles [11] of these ligands with those for the more widely studied triphenylphosphines. The Tolman cone angle comparisons are based on the crystallographic data rather than the mechanical model procedures first described by Tolman, and in particular the conformations of the ligands actually observed in the structures were used as the basis for the calculations.

For the determination of the Tolman cone angles, the coordinates of the atoms were read into a molecular editing program [12]. For the phosphines a hypothetical metal atom X was placed in a distance of 1.28 Å from the phosphorus atom, so that all X–P–C angles were equal. For the coordinated complexes the distance from the phosphorus to the metal centre was adjusted to 1.28 Å. The half-angle θ_i was then mea-

Table 4
Selected bond lengths (Å) and angles (°) for 4

Au(1)–P(1)	2.274(4)	Fe(2)–C(23)	2.035(19)
Au(1)–C(1)	2.011(15)	Fe(2)–C(24)	2.055(17)
Fe(1)–C(11)	2.020(12)	Fe(2)–C(25)	2.034(16)
Fe(1)–C(12)	2.017(13)	Fe(2)–C(26)	2.035(17)
Fe(1)–C(13)	2.031(16)	Fe(2)–C(27)	2.042(19)
Fe(1)–C(14)	2.027(17)	Fe(2)–C(28)	2.029(21)
Fe(1)–C(15)	2.028(14)	Fe(2)–C(29)	2.015(27)
Fe(1)–C(16)	1.987(20)	Fe(2)–C(30)	2.024(20)
Fe(1)–C(17)	2.005(21)	P(1)–C(11)	1.817(14)
Fe(1)–C(18)	2.032(17)	P(1)–C(21)	1.790(13)
Fe(1)–C(19)	2.035(15)	P(1)–C(31)	1.813(13)
Fe(1)–C(20)	1.976(21)	C(1)–C(2)	1.172(21)
Fe(2)–C(21)	2.029(15)	C(2)–C(3)	1.478(22)
Fe(2)–C(22)	2.035(15)		
P(1)–Au(1)–C(1)	174.3(4)	C(2)–C(3)–C(8)	119.1(14)
Au(1)–P(1)–C(11)	115.5(4)	Fe(1)–C(11)–P(1)	128.6(7)
Au(1)–P(1)–C(21)	109.9(5)	P(1)–C(11)–C(12)	126.0(10)
C(11)–P(1)–C(21)	104.8(6)	P(1)–C(11)–C(15)	126.6(10)
Au(1)–P(1)–C(31)	117.9(4)	Fe(2)–C(21)–P(1)	125.8(8)
C(11)–P(1)–C(31)	102.6(6)	P(1)–C(21)–C(22)	123.8(11)
C(21)–P(1)–C(31)	104.9(6)	P(1)–C(21)–C(25)	129.6(12)
Au(1)–C(1)–C(2)	176.9(13)	P(1)–C(31)–C(32)	120.8(10)
C(1)–C(2)–C(3)	179.4(15)	P(1)–C(31)–C(36)	120.5(10)
C(2)–C(3)–C(4)	121.0(16)		

sured for each substituent on the phosphorus atom as the angle between the phosphorus centre, the metal atom and the hydrogen atom on the substituent which gives the largest value for the angle θ_i (Fig. 10). The Tolman cone angle Θ is then calculated as two thirds of the sum of the half-angles θ_i.

The method we used differs from Tolman's method. We used the atomic centres instead of the surfaces of the van der Waals spheres of the atoms in the substituents to determine the cone angle. Thus the distance from the phosphorus atom to the metal atom has had to be reduced by the van der Waals radius of hydrogen (1.00 Å) to 1.28 Å. Geometrically the two methods are strictly equivalent only for a cone angle of 180°. The difference between the two methods increases when angles are far from 180°; cone angles for $\Theta \neq 180°$ are calculated to be smaller than those obtained using Tolman's definition.

Table 1 gives the values for the calculated cone angles and the average X–P–C and Au–P–C angles for the naphthyl- and ferrocenyl-substituted phosphine and for the literature PPh_3 and P(*m*-Tol)$_3$ compounds. Within the free phosphines the average X–P–C angle increases from PPh_3, P(*m*-Tol)$_3$, $PFcPh_2$ to PFc_2Ph, consistent with the increasing bulk of the substituent. Similarly the cone angles for the free phosphines increase in parallel from 152°, 159°, 165° to 190°, respectively. It is interesting to note that, contrary to expectation, as the bulk of the phosphine increases the C–P–C angles contract and the average X–P–C angle increases.

On coordination the proportion of s character in the P–C bond increases, and the angle between the substituents on P opens up, resulting in a lower average Au–P–C angle. The angle X–P–C for PPh_3 changes coordination to the Au–C≡C–Au unit from 115.6° to 112.8°. Similarly, the angles for P(*m*-Tol)$_3$ changes from 116.4° to 112.6° and for PFc_2Ph the angle decreases from 117.9° to 115.2°. As a result, the cone angles calculated using the coordinated complexes are larger than those calculated for the free phosphines.

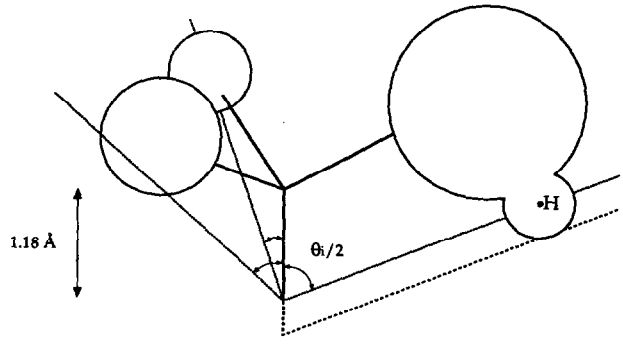

Fig. 10. Method of measuring cone angles.

Table 5
Average angles X–P–C and Au–P–C and calculated cone angles (°) for coordinated phosphines of the type R_3P–Au–C≡C–Au–PR_3 and for the free phosphines

Compound	Average Au–P–C	Cone angle calculated as part of this study	Ligand	Average X [a]–P–C angle in the free phosphine	Cone angle of the free phosphine
[b]	112.8	162	PPh_3 [19]	115.6	152
[c]	112.6	165	P(*m*-Tol)$_3$ [20]	116.4	159
1	113.4	168	$PNpPh_2$		
2	113.1	177	PNp_2Ph		
			$PFcPh_2$ [21]	117.0	165
3	115.2	191	PFc_2Ph [22]	117.9	190

[a] X is an imaginary atom in direction of the lone pair with all X–P–C angles being equal.
[b] Ph_3P–Au–C≡C–Au–PPh_3.
[c] (*m*-Tol)$_3$P–Au–C≡C–Au–P(m-Tol)$_3$.

The angles calculated for PPh_3 and P(*m*-Tol)$_3$ in the ethyne complex are 162° and 165°, respectively. The cone angles of the $PNpPh_2$ complex (168°) and the PNp_2Ph complex (177°) increases only slightly relative to the cone angle in the PPh_3 complex, because the additional phenyl ring of the naphthyl group is able to tuck into empty space within the cone. The introduction of two bulky ferrocenyl groups leads relative to PPh_3 to a sharp increase of the cone angle to 191°. This is probably due to the inability of this group to tuck into the space within the cone.

2.7. Photophysical properties

The ethynyl–gold(I) complexes are of particular interest because of the presence of coordinatively unsaturated metal centres. Their lowest electronic excited states are usually long-lived and powerful reductants. This particular series of compounds was of interest because of the additional conjugation associated with the ethynyl fragment and the absence of intermolecular gold–gold interactions in the solid state.

The electronic absorption spectra of the complexes [Np_3P–Au–C≡C–Au–PNp_3] (7), [Np_2PhP–Au–C≡C–Au–$PPhNp_2$] (2) and [$NpPh_2P$–Au–C≡C–Au–PPh_2Np] (1) in CH_2Cl_2 show an intense absorption band at ca. 296 nm that is vibronically structured with progressional spacings typical of aromatic C–C vibrations. Similar absorption bands typical of the $n \rightarrow \pi^*$(Np) transitions (sometimes designated as $1 \rightarrow a_\pi$ transition) of aryl–phosphine ligands are also observable in the free ligands [13]. This type of transition involves the promotion of an electron from the lone-pair orbital (l) on phosphorus to an empty antibonding orbital of π origin (a_π) situated on the aryl ring. A comparison of the spectroscopic data [Ph_3P–Au–C≡C–Au–PPh_3] (8) with those for the monomeric

[Ph_3P–Au–C≡C–Ph] (**5**) shows that the $\sigma \rightarrow \pi^*$(Ph) transition of **5** is of lower energy than that of **8**, consistent with the higher electron density of the Au–P bond in **5** that **8** ($^{31}P\{^1H\}$ NMR: **5**, δ 42.6; **8**, δ 43.4). It is possible to visualize the dimeric complex **8** as a monomeric species with the phenyl substituent on C≡C in **5** replaced by the more electron-deficient $AuPPh_3$ unit. It is likely that in **8**, the more electron-deficient Ph_3P–Au–C≡C$^-$ moiety (compared with Ph–C≡C$^-$) has a better π-accepting ability, which would enhance metal to ligand back π bonding (d_π(Au) → π*(Ph_3P–Au–C≡C$^-$)) between the Au and C atoms, leaving less d_π(Au)–3d(P) overlap and resulting in a smaller effective synergistic effect on the Au–P bond.

Excitation of solid sample or fluid solution of the complexes at $\lambda > 330$ nm resulted in intense long-lived luminescence. The photophysical data are summarized in Table 6. The long lifetime of the emission suggests that the emission is most likely associated with a spin-forbidden transition. Similar phosphorescent bands are also observable upon visible-light excitation of the free ligands. With reference to previous spectroscopic work on d^{10} metal phosphine complexes and phosphine ligands [13], the phosphorescent state is likely to be derived from the $\sigma \rightarrow \pi^*$(Np) transition (sometimes designated as $\sigma \rightarrow a_\pi$ transition) for the complexes analogous to the n → π*(Np) assignment for the corresponding phosphine ligands. Upon coordination of the phosphine molecule, the electron pair that formerly resided in the l orbital now engages in σ bonding to the metal atom. Accordingly, the transition involves the transfer of an electron from this σ orbital to the a_π orbital of the aryl ring. The observation that the emission energies for the complexes are in the order **7** < **2** < **1** < **8** is in agreement with the $\sigma \rightarrow \pi^*$(Ar) transition assignment. This is also in accord with $^{31}P\{^1H\}$ NMR data (**2**, δ 30.7; **1**, δ 38.0; **8**, δ 43.4), since the electron density around the P atom should be highest for **7** and lowest for **8**. Thus the σ electrons of the Au–P bond in **7** would be most readily available for donation to the low-lying empty π*(Np) orbital relative to **2** and **1**, resulting in the lowest $\sigma \rightarrow \pi^*$(Np) transition energy for **7**. For **8**, since the downfield ^{31}P NMR shift would lower the σ energy level and replacing the naphthyl group by a phenyl group would raise the π*(Ar) energy level (π*(Np) < π*(Ph)), the $\sigma \rightarrow \pi^*$(Ph) transition would be highest in energy. The introduction of ferrocenyl substituents on the phosphine ligand in [Fc_2PhP–Au–C≡C–Au–PFc_2Ph] (**3**) and [Fc_2PhP–Au–C≡C–Ph] (**4**) causes the luminescence quantum yield and lifetime to be much reduced. It is possible that the ferrocenyl group quenches the emissive state via intramolecular reductive electron transfer processes. A comparison of the luminescent behaviour of the monomeric complexes of **5** and [$MePh_2PAuC{\equiv}CPh$] (**6**) shows that the emission energy of the latter is shifted to lower energy ($\sigma \rightarrow \pi^*$(Ph) transition), consistent with the electron richness of the Au–P σ bond. The monomeric [$BpPh_2P$–Au–C≡CH] (**10**) also shows similar luminescent behaviour.

Table 6
Photophysical data for the gold complexes and phosphine ligands

Compound	Medium (T/K)	λ_{em}/nm[a]	$\tau_0/\mu s$
1	Solid (298)	459, 556sh	0.55, 2.85
	Solid (77)	450sh, 547	
	CH_2Cl_2 (298)	420, 519	82.0
	$CHCl_3$ (77)	420, 523	
2	Solid (298)	481, 552sh	0.45
	Solid (77)	480sh, 556	
	CH_2Cl_2 (298)	521	17.0
	$CHCl_3$ (77)	523	
3	Solid (298)	432, 544	0.23
	Solid (77)	424, 520	
	CH_2Cl_2 (298)	402, 462sh	
4	Solid (298)	430, 558	0.23
	Solid (77)	426, 520	
	CH_2Cl_2 (298)	414, 482sh	
5	Solid (298)	459	33.4
	Solid (77)	457	
	CH_2Cl_2 (298)	410, 454sh	6.6
6	Solid (298)	524	3.4
	Solid (77)	477	
	CH_2Cl_2 (298)	426, 454	3.4
7	Solid (298)	483, 555sh	0.80
	Solid (77)	482sh, 554	
8	Solid (298)	530	1.3, 5.4
	Solid (77)	523	
	CH_2Cl_2 (298)	469, 610	6.4, 7.6
	$CHCl_3$ (77)	468, 526	
10	Solid (298)	420sh, 545	1.3, 6.3
	Solid (77)	488	
	CH_2Cl_2 (298)	484	0.4
	$CHCl_3$ (77)	480	
PNp_3	Solid (298)	590	0.3
	Solid (77)	490, 524	
PNp_2Ph	Solid (298)	495	0.3
	Solid (77)	486, 566	
	CH_2Cl_2 (298)	534	
	$CHCl_3$ (77)	486, 524, 562	
$PNpPh_2$	Solid (298)	455	0.3
	Solid (77)	445	
	CH_2Cl_2 (298)	538	
	$CHCl_3$ (77)	485, 520	
PFc_2Ph	Solid (298)	422, 573	0.2
	Solid (77)	424, 516	
	CH_2Cl_2 (298)	404, 490sh	

[a] Excitation wavelength at 350 nm.

A similar emission trend is observable for the free phosphine ligands. Np_3P which exhibits the most upfield ^{31}P NMR shift, displays the lowest energy emission. On the other hand, $NpPh_2P$, which has the most downfield ^{31}P chemical shift, exhibits the highest energy emission among the three naphthyl-substituted phosphines. All these are consistent with the assignment of the emission originating from an n → π*(Np) transition where Np_3P would have its n orbital highest in energy (most electron-rich lone pair on P atom), and

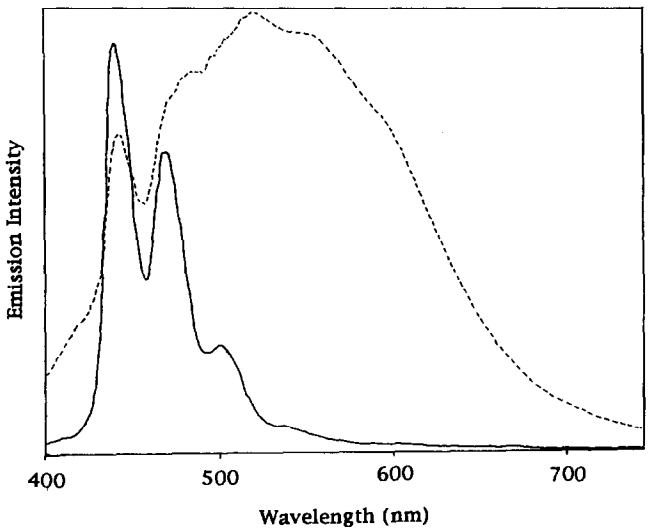

Fig. 11. Room-temperature emission spectra of complex **2** in degassed dichloromethane with excitation wavelength at 350 nm (dashed line) and 380 nm (solid line).

hence a narrower $n \rightarrow \pi^*(Np)$ energy gap given the almost identical $\pi^*(Np)$ level for all three phosphines.

An noteworthy feature associated with the solution luminescence of complex **2** is that the emission spectra displayed multiple luminescence, strongly dependent on the excitation wavelength (Fig. 11). Excitation of a degassed dichloromethane solution of **2** at $\lambda = 350$ nm at room temperature resulted in a broad, structureless emission band centred at ca. 520 nm. On the other hand, excitation of the same solution at $\lambda = 380$ nm resulted in a rich vibronically structured emission band in the 440–540 nm region with progressional spacing of ca. 1220–1400 cm^{-1}, typical of aromatic C–C vibrations. It is likely that the 520 nm band that is at lower energy is $\sigma \rightarrow \pi^*(Np)$ in nature while the higher energy vibronic band in the 440–540 nm region is $\pi \rightarrow \pi^*(Np)$ in origin. This is also consistent with the larger Stokes shift expected for the $\sigma \rightarrow \pi^*(Np)$ emission, which involves removal of an electron from a σ Au–P bonding orbital to an essentially ligand-centred π^* antibonding orbital, resulting in a larger structural distortion of the excited-state molecule relative to the ground state. Moreover, a comparison of the solution emission spectra of **2** and its corresponding free phosphine ligand, Np_2PhP, shows that the emission maximum of **2** (521 nm) is at higher energy than that of Np_2PhP (534 nm), consistent with the $\sigma \rightarrow \pi^*(Np)$ origin for the former and the $n \rightarrow \pi^*(Np)$ origin assignment for the latter, since the σ electrons would be expected to be less available for donation to the $\pi^*(Np)$ orbital than the lone pair electrons on the free ligand.

3. Experimental

3.1. General

Standard Schlenk techniques and a nitrogen atmosphere were used routinely for carrying out reactions, but no special precautions were taken to exclude oxygen during work-up procedures, unless stated otherwise. Solvents were of reagent grade and were dried by standard methods [14] and distilled under N_2.

3.2. Physical measurements and instrumentation

Infrared spectra were recorded on a Perkin-Elmer 1720 Fourier transform infrared spectrometer as KBr pellets. Raman spectra were obtained on a Perkin-Elmer NIR FT-Raman 1700X spectrometer equipped with an Nd:YAG laser (1064 nm). UV–visible spectra were obtained on a Milton Roy Spectronic 3000 diode-array spectrophotometer. Steady-state excitation and emission spectra were obtained on a Spex Fluorolog-2 111 spectrofluorimeter. Low-temperature (77 K) spectra for solid samples and $CHCl_3$ glass matrices were recorded by using an optical Dewar sample holder. ^1H, $^{31}P\{^1H\}$ and $^{13}C\{^1H\}$ NMR spectra were recorded on a JEOL JNM-GSX270 and on a JEOL JNM-EX270 Fourier transform NMR spectrometer with chemical shifts reported relative to TMS and H_3PO_4, respectively.

Emission-lifetime measurements were performed using a conventional laser system. The excitation source was the 355 nm output (third harmonic) of a Quanta-Ray Q-switched DCR-3 pulsed Nd:YAG laser (10 Hz, G-resonator). Luminescence decay signals were recorded on a Tektronix Model 2430 digital oscilloscope and analysed using a program for exponential fits. All solutions for photophysical studies were prepared under vacuum in a 10 cm^3 round-bottomed flask equipped with a side-arm 1 cm fluorescence cuvette and sealed from the atmosphere by a Kontes quick-release Teflon stopper. Solutions were rigorously degassed with no fewer than four freeze–pump–thaw cycles.

3.3. Synthesis of the phosphines

The phosphines were prepared by modification of published methods [15], with carefull exclusion of oxygen during all steps to minimize the oxidation to phosphine–oxide. Triphenylphosphine and diferrocenylphenylphosphine were obtained from Aldrich.

Np_3P

$^{31}P\{^1H\}$ NMR ($CDCl_3$): δ −32.4. UV–visible (CH_2Cl_2)/nm (ε/dm^3 mol^{-1} cm^{-1}): 239 (23 800), 293 (16 800), 306sh (15 500), 316sh (14 300), 326sh (12 100).

Np_2PhP

$^{31}P\{^1H\}$ NMR ($CDCl_3$): δ −22.5. UV–visible (CH_2Cl_2)/nm (ε/dm^3 mol^{-1} cm^{-1}): 238 (22800), 307 (10600), 315sh (9700), 323sh (7300).

$NpPh_2P$

$^{31}P\{^1H\}$ NMR ($CDCl_3$): δ −12.8. UV–visible (CH_2Cl_2)/nm (ε/dm^3 mol^{-1} cm^{-1}): 236 (15600), 283 (8300), 300sh (7700).

Fc_2PhP

$^{31}P\{^1H\}$ NMR ($CDCl_3$): δ −29.2. UV–visible (CH_2Cl_2)/nm (ε/dm^3 mol^{-1} cm^{-1}): 252sh (18600), 314sh (2420), 432sh (500).

3.4. Synthesis of the chlorophosphinegold(I) complexes

Np_3PAuCl

A solution of the phosphine (0.412 g, 1.0 mmol) in CH_2Cl_2 (20 cm^3) was added during 5 min to a magnetically stirred solution of $Au(SMe_2)Cl$ [16] (0.295 g, 1.0 mmol) in CH_2Cl_2 (20 cm^3). The complex was precipitated by addition of hexane, and dimethyl sulphide and dichloromethane were removed under a partial vacuum. The product was filtered off, recrystallized from dichloromethane/hexane and dried in vacuo.

Yield: 91%. Found: C, 51.1; H, 2.9%. Calc. for $C_{30}H_{21}AuClP$: C, 51.0; H, 3.2% $^{31}P\{^1H\}$ NMR ($CDCl_3$): δ (s) 7.0. ^1H NMR ($CDCl_3$): δ 7.2–8.8 (m). IR: 337 cm^{-1}, ν(AuCl).

$Np_2PhPAuCl$

Yield: 94%. Found: C, 51.5; H, 3.3%. Calc. for $C_{26}H_{19}AuClP$: C, 52.1; H, 2.8% $^{31}P\{^1H\}$ NMR ($CDCl_3$): δ 17.4 (s). ^1H NMR ($CDCl_3$): δ 7.0–8.7 (m). IR: 331 cm^{-1}, ν(AuCl).

$NpPh_2PAuCl$

Yield: 86%. Found: C, 48.3; H, 2.8%. Calc. for $C_{22}H_{17}AuClP$: C, 48.5; H, 3.1% $^{31}P\{^1H\}$ NMR ($CDCl_3$): δ 26.9 (s). ^1H NMR ($CDCl_3$): δ 7.0–8.4 (m). IR: 327 cm^{-1}, ν(AuCl).

$Fc_2PhPAuCl$

Yield: 51%. Found: C, 43.7; H, 3.1%. Calc. for $C_{26}H_{23}AuClFe_2P$: C, 43.9; H 3.2%. $^{31}P\{^1H\}$ NMR ($CDCl_3$): δ 24.0 (s). ^1H NMR ($CDCl_3$): δ 7.4–7.8 (m, 5H), 4.2–4.5 (m, 18H). IR: 329 cm^{-1}, ν(AuCl).

$BpPh_2PAuCl$

Yield: 77%. Found: C, 50.2; H, 3.3%. Calc. for $C_{24}H_{19}AuClP$; C, 50.5; H, 3.3% $^{31}P\{^1H\}$ NMR ($CDCl_3$): δ 33.3 (s). ^1H NMR ($CDCl_3$): δ 7.36–7.72 (m). IR: 329 cm^{-1}, ν(AuCl).

3.5. Synthesis of ethynyl–gold (I) complexes

3.5.1. *[$Np_3PAuCCAuPNp_3$] (7)*

A solution of Np_3PAuCl (0.288 g, 0.446 mmol) in THF (20 cm^3) was filtered into a magnetically stirred solution of KO^{t}Bu in ethanol (30 cm^3). Ethyne was bubbled through the resulting colloidal suspension. The reaction was monitored by IR spectroscopy, and as soon as the ν(Au–Cl) had disappeared it was stopped by removing any excess ethyne by application of a weak vacuum. The solvent was reduced until a precipitate separated. The precipitate was filtered off and then stirred with methanol (100 cm^3) overnight, washed with a small volume of dichloromethane (5 cm^3) and dried in vacuo.

Yield: 0.113 g, 41%. Found: C, 57.5; H, 3.3%. Calc. for one CH_2Cl_2 solvent molecule, $C_{64}H_{44}Au_2Cl_2P_2$: C, 57.9; H, 3.3%. Raman: 2008 cm^{-1} vs, ν(C≡C). UV–visible (CH_2Cl_2)/nm: 230, 287, 297, 308sh. The NMR spectra and the extinction coefficients were not recorded owing to the very low solubility of the complex in organic solvents.

3.5.2. *[$Np_2PhPAuCCAuPNp_2Ph$] (2)*

A solution of $Np_2PhPAuCl$ (0.265 g, 0.45 mmol) in THF (5 cm^3) was filtered into a magnetically stirred solution of KO^{t}Bu (0.053 g, 0.45 mmol) in EtOH (30 cm^3). A stream of ethyne was passed through the colloidal solution until an intense white precipitate separated (5 min). A mild vacuum was applied and about 5 cm^3 of solvent removed. The precipitate was filtered off and then stirred overnight with MeOH/H_2O (1 : 1, 100 cm^3). The precipitate was again filtered off and dried over silica gel. Crystals suitable for X-ray analysis were obtained from a $CHCl_3$ solution by slow evaporation at −20°C.

Yield: 0.229 g, 90%. Found: C, 53.8; H, 3.3%. Calc. for one $CHCl_3$ solvent molecule, $C_{55}H_{39}Au_2Cl_3P_2$: C, 52.3; H, 3.1%. $^{31}P\{^1H\}$ NMR (CD_2Cl_2): δ 30.7 (s). ^1H NMR (CD_2Cl_2): δ 7.0–8.7 (m). Raman: 2012 cm^{-1} vs, ν(C≡C). UV–visible (CH_2Cl_2)/nm (ε/dm^3 mol^{-1} cm^{-1}): 232 (169000), 274 (35800), 284 (42500), 296 (51000), 306sh (36500), 315sh (20100), 322sh (10100).

3.5.3. *[$NpPh_2PAuCCAuPNpPh_2$] (1)*

The procedure as used for (2) was employed but the time of reaction with ethyne was reduced to 3 min. Crystals for X-ray analysis were obtained from a saturated solution in $CHCl_3$ at 4°C.

Yield: 0.204 g, 88%. Found: C, 52.3; H, 3.2%. Calc. for $C_{46}H_{34}Au_2P_2$: C, 53.0; H, 3.3%. $^{31}P\{^1H\}$ NMR (CD_2Cl_2): δ 38.0 (s). ^1H NMR (CD_2Cl_2): δ 6.9–8.4 (m). Raman 2007 cm^{-1} vs, ν(C≡C). UV–visible (CH_2Cl_2)/nm (ε/dm^3 mol^{-1} cm^{-1}): 230 (90500), 261 (20000), 284 (17400), 295 (19500), 306sh (12600), 318sh (4100).

3.5.4. [$Ph_3PAuCCAuPPh_3$] (8)

Compound **6** was prepared by the procedure described by **2**. On the addition of ethyne a precipitate separated instantly. The reaction was stopped after 1 min.

Yield: 0.150 g, 80%. Found: C, 46.4; H, 3.0%. Calc.

Table 7
Crystal and refinement data for **1–4**

Parameter	**1** $[NpPh_2PAuC]_2 \cdot 2CHCl_3$	**2** $[Np_2PhPAuC]_2 \cdot 6CHCl_3$	**3** $[Fc_2PhPAuC]_2 \cdot 4C_2H_6O$	**4** $Fc_2PhPAuCCPh$
(a) Crystal Data				
Chemical formula	$C_{48}H_{36}Au_2Cl_6P_2$	$C_{60}H_{44}Au_2Cl_{18}P_2$	$C_{62}H_{70}Au_2Fe_4O_4P_2$	$C_{34}H_{28}AuFe_2P$
Formula weight	1281.3	1858.9	1558.5	776.2
Crystal system	Monoclinic	Triclinic	Triclinic	Monoclinic
Unit cell dimensions				
a/Å	12.241(2)	11.989(6)	10.951(5)	12.141(7)
b/Å	10.932(2)	12.597(4)	11.368(5)	19.053(11)
c/Å	18.100(3)	14.263(4)	13.106(10)	12.458(8)
α/°		105.74(2)	69.08(5)	
β/°	100.21(2)	98.94(2)	79.41(5)	92.62(2)
γ/°		117.76(2)	75.31(4)	
V/Å^3	2383.7(7)	1731.4(12)	1466.4(14)	2879(3)
Space group	$P2_1/n$	$P\bar{1}$	$P\bar{1}$	$P2_1/a$
D_c/g cm^{-3}	1.785	1.783	1.765	1.791
Z	2	1	1	4
F(000)	1228	898	766	1512
Colour, habit	Colourless needles	Colourless prisms	Orange prisms	Orange plate prisms
Crystal dimensions, mm	0.10 × 0.10 × 0.50	0.13 × 0.13 × 0.16	0.16 × 0.16 × 0.23	0.10 × 0.33 × 0.46
μ, cm^{-1}	153.83	149.76	60.46	61.55
(b) Data collection and Processing				
Diffractometer	Siemens P4/PC	Siemens P4/PC	Siemens P4/PC	Siemens P4/PC
X-radiation	Cu Kα	Cu Kα	Mo Kα	Mo Kα
Scan mode	ω	ω	ω	ω
ω-scan width, deg	0.90	0.90	0.90	0.90
2θ limits, deg	0.0–116.0	3.0–120.0	3.0–50.0	3.0–50.0
Min., max. h, k, l	0, 13; 0, 12; −19, 19	−11, 13; −14, 12; −10, 16	0, 13; −12, 13; −15, 15	0, 14; 0, 22; −14, 14
No. of reflections	3484	5119	5160	5310
Total				
Unique (R_{int}/%)	3318 (3.39)	5119	5160	5065 (2.09)
Observed	2821 ($F > 4.0\sigma(F)$)	4471 ($F > 4.0\sigma(F)$)	4548 ($F > 3.0\sigma(F)$)	3486 ($F > 4.0\sigma(F)$)
Absorption correction	Face-indexed numerical	Semi-empirical	Semi-empirical	Face-indexed numerical
Min., max. transmissions	0.1134, 0.4062	0.2705, 0.4816	0.2101, 0.3687	0.2241, 0.6883
(c) Structure Analysis and Refinement				
No. of parameters	263	371	334	344
Weighting scheme	$w^{-1} = \sigma^2(F) + 0.0005F^2$	$w^{-1} = \sigma^2(F) + 0.0005F^2$	$w^{-1} = \sigma^2(F) + 0.0005F^2$	$w^{-1} = \sigma^2(F) + 0.0005F^2$
Extinction correction, $F^* = F[1 + 0.002\chi F^2/\sin(2\theta)]^{-1/4}$	$\chi = 0.00055(9)$	$\chi = 0.0018(3)$	N/A	$\chi = 0.00056(5)$
R (observed data), %	3.72	6.09	3.57	4.57
R_w (observed data), %	4.06	6.48	3.64	4.09
Goof	1.53	2.73	1.57	1.84
Largest and mean Δ/σ	0.003, 0.001	0.015, 0.002	0.060, 0.004	0.048, 0.006
Data-to-parameter ratio	10.7:1	12.1:1	13.6:1	10.1:1
Min., max. residual density, e Å^{-3}	1.46, −0.64	1.70, −2.18	1.18, −0.84	1.50, −0.68

for two H_2O solvent molecules, $C_{38}H_{34}Au_2O_2P_2$: C, 46.6; H, 3.5. $^{31}P\{^1H\}$ NMR (CD_2Cl_2): δ 43.4 (s). ^1H NMR (CD_2Cl_2): δ 7.3–7.6 (m). $^{13}C\{^1H\}$ NMR (CD_2Cl_2): δ 134.2 (d, J_{CP} = 13.4 Hz), 131.1 (s), 128.8 (d, J_{CP} = 11 Hz). Raman: 2002 cm^{-1} vs, ν(C≡C). UV–visible (CH_2Cl_2)/nm (ε/dm^3 mol^{-1} cm^{-1}): 234 (48 800), 265 (18 800), 288sh (4150).

3.5.5. [$Fc_2PhPAuC{\equiv}CAuPPhFc_2$] (3)

The compound was prepared by the procedure described for **2**. The time of reaction with ethyne was 2 h. The complex was recrystallized from CH_2Cl_2/ethanol. Crystals suitable for X-ray analysis were obtained by layering a CH_2Cl_2 solution of **3** with ethanol.

Yield: 0.197 g, 68%. Found: C, 47.8; H, 3.4%. Calc. for $C_{54}H_{46}Au_2Fe_4P_2$: C, 47.3 H, 3.2% $^{31}P\{^1H\}$ NMR (CD_2Cl_2): δ 31.4 (s). ^1H NMR (CD_2Cl_2): δ 7.9–8.0 (m, 4H), 7.4 (s, 6H), 4.3–4.5 (dd, 8H), 4.2 (s, 20H). $^{13}C\{^1H\}$ NMR (CD_2Cl_2): δ 145.0 (dd, J^1_{CP} = 136 Hz, J^2_{CP} = 21 Hz), 128.2–134.3 (mm), 70.9–73.7 (m), 69.9 (s). Raman: 2003 cm^{-1} vs, ν(C≡C). UV–visible (CH_2Cl_2)/nm (ε/dm^3 mol^{-1} cm^{-1}): 242 (63 800), 258 (58 200) 270sh (27 300), 285sh (15 600), 300sh (10 400), 406br (5170).

Table 8
Atomic coordinates ($\times 10^4$) and equivalent isotropic displacement coefficients ($Å^2 \times 10^3$) for complex **1**

	x	y	z	U(eq) [a]
Au(1)	−1041(1)	3568(1)	−4218(1)	54(1)
P(1)	−1877(2)	2161(2)	−3576(1)	51(1)
C(1)	−271(7)	4694(7)	−4815(4)	55(3)
C(11)	−1483(6)	607(7)	−3776(4)	54(3)
C(12)	−985(8)	−137(7)	−3197(5)	65(3)
C(13)	−562(9)	−1299(8)	−3335(6)	79(4)
C(14)	−656(9)	−1688(9)	−4057(6)	79(4)
C(15)	−1172(8)	−1384(8)	−5400(6)	70(4)
C(16)	−1617(8)	−670(10)	−5986(5)	77(4)
C(17)	−2048(7)	490(9)	−5871(5)	69(4)
C(18)	−2038(7)	909(8)	−5159(4)	58(3)
C(19)	−1553(6)	188(7)	−4534(4)	51(3)
C(20)	−1148(7)	−981(7)	−4653(5)	55(3)
C(21)	−1544(8)	2303(8)	−2564(4)	60(3)
C(22)	−569(10)	2865(10)	−2266(6)	91(5)
C(23)	−264(14)	2886(14)	−1462(8)	134(7)
C(24)	−947(19)	2410(18)	−1028(8)	155(11)
C(25)	−1873(16)	1866(17)	−1336(8)	136(9)
C(26)	−2188(11)	1823(11)	−2103(6)	96(5)
C(31)	−3378(7)	2215(8)	−3783(4)	58(3)
C(32)	−3872(8)	3345(10)	−3814(5)	77(4)
C(33)	−5016(11)	3440(13)	−3927(7)	108(6)
C(34)	−5661(10)	2417(16)	−4022(6)	98(6)
C(35)	−5192(11)	1287(14)	−4005(7)	107(6)
C(36)	−4020(8)	1179(9)	−3889(6)	82(4)
C(41)	1810(8)	5224(9)	−3365(5)	80(4)
Cl(1)	2959(3)	6112(3)	−3448(3)	145(2)
Cl(2)	1072(3)	5920(3)	−2731(2)	115(1)
Cl(3)	2241(3)	3776(2)	−3037(2)	99(1)

[a] Equivalent isotropic U defined as one third of the trace of the orthogonalized U_{ij} tensor.

Table 9
Atomic coordinates ($\times 10^4$) and equivalent isotropic displacement coefficients ($Å^2 \times 10^3$) for complex **2**

	x	y	z	U(eq) [a]
Au(1)	2177(1)	628(1)	1327(1)	43(1)
P(1)	4099(4)	1086(3)	2424(3)	43(2)
C(1)	503(15)	139(15)	320(12)	51(8)
C(11)	5331(13)	1448(16)	1772(12)	53(8)
C(12)	5804(14)	573(16)	1542(12)	56(8)
C(13)	6658(16)	750(14)	951(14)	60(9)
C(14)	7024(18)	1689(18)	578(13)	68(10)
C(15)	6997(19)	3598(18)	436(15)	74(12)
C(16)	6614(17)	4460(19)	654(14)	73(11)
C(17)	5764(17)	4329(15)	1242(12)	60(10)
C(18)	5350(16)	3349(14)	1619(12)	62(8)
C(19)	5756(14)	2467(12)	1410(11)	44(7)
C(20)	6636(15)	2603(15)	826(12)	54(9)
C(21)	4875(14)	2432(13)	3676(10)	41(7)
C(22)	6208(16)	3390(15)	3985(11)	60(9)
C(23)	6844(20)	4445(18)	4929(12)	71(10)
C(24)	6162(19)	4546(16)	5573(12)	66(10)
C(25)	4096(23)	3652(19)	6016(15)	74(13)
C(26)	2785(27)	2719(25)	5766(16)	91(18)
C(27)	2135(22)	1661(21)	4789(15)	82(13)
C(28)	2763(15)	1565(16)	4107(13)	57(9)
C(29)	4126(16)	2513(15)	4362(11)	50(8)
C(30)	4797(19)	3589(16)	5332(11)	60(10)
C(31)	3907(15)	−282(14)	2730(10)	45(8)
C(32)	2755(16)	−1491(15)	2163(13)	61(9)
C(33)	2610(21)	−2564(17)	2359(15)	76(11)
C(34)	3570(23)	−2456(19)	3087(15)	84(13)
C(35)	4699(23)	−1258(22)	3653(16)	87(15)
C(36)	4881(19)	−142(18)	3503(13)	71(11)
C(2)	8439(21)	8930(18)	1751(15)	81(13)
Cl(1)	8711(11)	10192(8)	2767(6)	187(8)
Cl(2)	6776(8)	7799(7)	1139(7)	146(5)
Cl(3)	9239(7)	8185(7)	2173(6)	120(5)
C(3)	936(18)	3209(17)	1113(14)	72(10)
Cl(4)	547(7)	3561(9)	2205(5)	144(5)
Cl(5)	2657(6)	3950(7)	1375(5)	107(4)
Cl(6)	347(5)	3755(6)	246(5)	106(4)
C(4)	10964(26)	6984(24)	4426(21)	121(18)
Cl(7)	10807(8)	6859(7)	5596(6)	127(5)
Cl(8)	9457(8)	5857(7)	3408(6)	135(5)
Cl(9)	11473(8)	8566(7)	4532(6)	135(5)

[a] Equivalent isotropic U defined as one third of the trace of the orthogonalized U_{ij} tensor.

3.5.6. [$Ph_3PAuCCPh$] (5)

This was prepared by a published procedure [17]. $^{31}P\{^1H\}$ NMR (CD_2Cl_2): δ 42.6 (s). ^1H NMR (CD_2Cl_2): δ 7.2–7.6 (m). UV–visible (CH_2Cl_2)/nm (ε/dm^3 mol^{-1} cm^{-1}): 238 (32 000), 271 (19 400), 284 (19 300), 291sh (11 400).

3.5.7. [$MePh_2PAuCCPh$] (6)

This was prepared in the same way as [$Ph_3PAuCCPh$] but with PPh_3 replaced by $PMePh_2$. Reaction of [AuCCPh]$_x$ with one equivalent of $PMePh_2$ in benzene afforded [$MePh_2PAuCCPh$] in almost quantitative yield. Colourless crystals were obtained by recrystallization from CH_2Cl_2/light petroleum.

$^{31}P\{^1H\}$ NMR (CD_2Cl_2): δ 26.9 (s). ^1H NMR (CD_2Cl_2): δ 7.2–7.7 (m, 15H), 2.1 (d, $J_{PH} = 10$ Hz, 3H). UV–visible (CH_2Cl_2)/nm (ε/dm^3 mol^{-1} cm^{-1}): 232 (31 000), 237 (32 700), 259sh (15 200), 270 (25 900), 283 (27 100), 290sh (14 900), 296sh (7000).

3.5.8. [$Fc_2PhPAuC{\equiv}CPh$] (4)

To a suspension of $Fc_2PhPAuCl$ (0.25 g, 0.35 mmol) in ethanol were added PhC≡CH (0.04 ml, 0.35 mmol in ethanol) and NaOEt (freshly prepared from Na (0.08 g, 0.35 mmol) in ethanol) and the mixture was refluxed. During the heating the precipitate partially dissolved and then intensified again. After 1 h the mixture was cooled to 4°C and left overnight. The product was then filtered off.

Yield: 0.262 g, 96%. Found: C, 52.3; H, 3.5%. Calc. for $C_{34}H_{28}AuFe_2P$: C, 52.6; H, 3.6%. $^{31}P\{^1H\}$ NMR (CD_2Cl_2): δ 32.1 (s). UV–visible (CH_2Cl_2)/nm (ε/dm^3 mol^{-1} cm^{-1}): 234 (34 400), 258 (25 500), 268 (33 300), 282 (31 600), 312sh (6130), 400br (3770).

Table 10
Atomic coordinates (×10^4) and equivalent isotropic displacement coefficients (Å^2 ×10^3) for complex **3**

	x	y	z	U(eq) [a]
Au(1)	1912(1)	8367(1)	5967(1)	46(1)
Fe(1)	2254(1)	4320(1)	7091(1)	48(1)
Fe(2)	2874(1)	8171(1)	9004(1)	58(1)
P(1)	3481(1)	6883(1)	6922(1)	38(1)
C(1)	443(6)	9618(7)	5212(6)	60(1)
C(11)	3655(5)	5270(5)	6937(5)	39(1)
C(12)	3721(5)	4855(6)	6017(5)	51(1)
C(13)	3912(6)	3509(7)	6372(7)	63(1)
C(14)	3927(6)	3052(6)	7515(7)	62(1)
C(15)	3773(5)	4144(5)	7871(6)	50(1)
C(16)	520(6)	5511(7)	7139(8)	75(1)
C(17)	692(7)	4968(10)	6298(8)	100(1)
C(18)	902(8)	3627(9)	6768(9)	96(1)
C(19)	838(7)	3363(8)	7863(9)	92(1)
C(20)	605(7)	4515(8)	8106(7)	75(1)
C(21)	3228(5)	6731(5)	8345(5)	42(1)
C(22)	2025(7)	6789(7)	8985(6)	62(1)
C(23)	2222(7)	6605(7)	10088(6)	69(1)
C(24)	3533(7)	6424(7)	10130(6)	64(1)
C(25)	4139(6)	6498(6)	9054(6)	51(1)
C(26)	2684(10)	9902(7)	7799(8)	99(1)
C(27)	1691(10)	9913(8)	8523(10)	114(1)
C(28)	2080(11)	9644(8)	9560(9)	116(1)
C(29)	3370(10)	9528(8)	9400(9)	106(1)
C(30)	3725(10)	9695(8)	8328(9)	101(1)
C(31)	5091(5)	7151(6)	6508(5)	42(1)
C(32)	5300(7)	8394(6)	6071(6)	65(1)
C(33)	6525(7)	8595(7)	5768(7)	79(1)
C(34)	7547(7)	7591(8)	5913(7)	77(1)
C(35)	7344(6)	6326(8)	6373(7)	74(1)
C(36)	6103(6)	6118(6)	6652(6)	55(1)
O(41)	1115(11)	9544(11)	2791(9)	132(1)
C(41)	2270(14)	8668(13)	3007(12)	196(1)
C(42)	2088(14)	7419(11)	3034(14)	125(1)
O(51)	975(10)	12049(13)	1283(13)	168(1)
C(51)	2020(12)	12626(14)	1138(13)	148(1)
C(52)	3184(12)	11935(14)	698(13)	167(1)

[a] Equivalent isotropic U defined as one third of the trace of the orthogonalized U_{ij} tensor.

Table 11
Atomic coordinates (×10^4) and equivalent isotropic displacement coefficients (Å^2 ×10^3) for complex **4**

	x	y	z	U(eq) [a]
Au(1)	1155(1)	1746(1)	3807(1)	43(1)
Fe(1)	−380(2)	1392(1)	675(2)	37(1)
Fe(2)	2086(2)	−392(1)	4015(2)	44(1)
P(1)	1820(3)	1076(2)	2472(3)	35(1)
C(1)	439(12)	2274(7)	4986(12)	47(5)
C(2)	−22(13)	2565(7)	5662(12)	52(5)
C(3)	−606(14)	2938(8)	6507(12)	51(6)
C(4)	−29(17)	3268(11)	7347(16)	97(9)
C(5)	−553(25)	3606(16)	8150(22)	148(14)
C(6)	−1636(30)	3611(16)	8129(21)	141(15)
C(7)	−2253(19)	3317(12)	7343(22)	110(11)
C(8)	−1732(15)	2948(8)	6457(15)	65(7)
C(11)	1221(10)	1246(6)	1134(11)	37(4)
C(12)	1053(11)	1927(7)	650(13)	48(5)
C(13)	637(12)	1819(9)	−399(13)	58(6)
C(14)	548(12)	1111(10)	−568(13)	61(6)
C(15)	887(10)	741(8)	360(12)	45(5)
C(16)	−1307(15)	1571(18)	1919(16)	111(13)
C(17)	−1547(15)	2056(11)	1139(22)	86(9)
C(18)	−1930(13)	1723(11)	250(16)	75(8)
C(19)	−1943(12)	1019(10)	441(16)	66(7)
C(20)	−1534(14)	908(11)	1464(21)	83(9)
C(21)	1535(12)	170(7)	2715(12)	50(5)
C(22)	633(11)	−69(8)	3300(16)	71(7)
C(23)	677(16)	−810(9)	3338(16)	81(8)
C(24)	1577(17)	−1036(8)	2765(14)	70(7)
C(25)	2112(14)	−442(7)	2386(12)	58(6)
C(26)	3065(15)	192(9)	5040(14)	66(7)
C(27)	2219(18)	−85(12)	5586(15)	88(9)
C(28)	2286(28)	−809(14)	5510(15)	119(13)
C(29)	3168(24)	−966(13)	4921(21)	110(12)
C(30)	3664(16)	−349(14)	4611(15)	88(9)
C(31)	3288(10)	1110(6)	2264(11)	37(4)
C(32)	3715(11)	837(8)	1342(12)	52(6)
C(33)	4824(13)	840(9)	1210(15)	71(7)
C(34)	5526(13)	1133(9)	1958(16)	71(7)
C(35)	5110(12)	1426(8)	2862(15)	60(6)
C(36)	3994(11)	1423(7)	3009(12)	43(5)

[a] Equivalent isotropic U defined as one third of the trace of the orthogonalized U_{ij} tensor.

3.5.9. [$NpPh_2PAuCCH$] (9)

The way prepared by the procedure described for **1**. The time of reaction with ethyne was increased to 2 h. The product was recrystallized from CH_2Cl_2/hexane.

Yield: 54%. Found: C, 48.8; H, 3.2%. Calc. for one CH_2Cl_2 solvent molecule, $C_{25}H_{20}AuCl_2P$: C, 48.5; H, 3.2%. $^{31}P\{^1H\}$ NMR (CD_2Cl_2): δ 40.3 (s). $^{13}C\{^1H\}$ NMR (CD_2Cl_2): δ 125.6–135.5 (m), δ 90.8 (s).

3.5.10. [$BpPh_2PAuCCH$] (10)

A suspension of $BpPh_2PAuCl$ (1.543 g, 2.71 mmol) in THF (20 cm^{-1}) was filtered into a magnetically

stirred solution of KO^{t}Bu (0.320 g, 2.71 mmol) in EtOH (20 cm^{-1}). Ethyne was bubbled through the stirred solution. An initially yellow precipitate separated and gradually turned white. After 24 h the reaction was stopped and the volume of the solution was reduced to 10 cm^3. The product was filtered off, washed with EtOH (100 cm^3) and recrystallized from CH_2Cl_2/hexane.

Yield: 1.334 g, 90%. Found: C, 55.3; H, 3.6%. Calc. for $C_{50}H_{38}Au_2P_2$: C, 54.8; H, 3.5%. $^{31}P\{^1H\}$ NMR (CD_2Cl_2): δ 42.0 (s). ^1H NMR (CD_2Cl_2): δ 7.4–7.7 (m, 19H) 1.8 (s, 1H). $^{13}C\{^1H\}$ NMR (CD_2Cl_2): δ 127.1–144.3 (m), 89.9 (s). UV–visible (CH_2Cl_2)/nm (ε/dm^3 mol^{-1} cm^{-1}): 230 (31 800), 272 (35 700).

3.6. Crystal structure determinations

The crystal data and refinement parameters for **1–4** are summarized in Table 7. The crystals were obtained as described above, and were mounted on glass fibres. Compounds **2** and **3** were sealed in Araldite to protect them from solvent loss.

The structures of **1**, **2** and **4** were solved by the heavy atom method and that of **3** by direct methods. Positional and anisotropic thermal parameters for non-hydrogen atoms were refined by full-matrix least-squares. Hydrogen atoms were introduced in calculated positions with C–H = 0.96 Å and assigned isotropic thermal parameters $U(H) = 1.2U_{eq}$ (C) and allowed to ride on their parent carbon atoms. The $CHCl_3$ solvent molecules in **1** and **2** display some rotational disorder, which accounts for their increased thermal parameters. The geometry of the ethanol molecules of **3** was constrained to O–C(1) = 1.417 ± 0.020 Å, C(1)–C(2) = 1.53 ± 0.02 Å and O–C(2) = 2.431 ± 0.020 Å. The hydrogens attached to the oxygen atoms could not be located. The crystal was partially desolvated and occupancies of all atoms in ethanol were estimated as 50%. All calculations were performed on a VAX station 3100 model 76 computer and on 386 and 486 PCs using the SHELXTL software package [18].

Atoms coordinates are listed in Tables 8–11. Full lists of bond lengths and angles and tables of thermal parameters and hydrogen atom coordinates have been deposited with the Cambridge Crystallographic Data Centre.

Acknowledgements

BP is thanked for their generous endowment to Imperial College and SERC for funding for the diffractometers. V.W.-W.Y. acknowledges financial support from the Research Grants Council and the University of Hong Kong. S.W.K.C. acknowledges the receipt of a postgraduate studentship administered by the University of Hong Kong.

References

[1] M.I. Bruce, K.R. Grundy, M.J. Liddell, M.R. Snow and E.R.T. Tiekink, *J. Organomet. Chem., C49* (1988) 344.
[2] D. Braga, A. Rodger and B.F.G. Johnson, *Inorg. Chim. Acta, 172* (1990) 185.
[3] D. Braga, F. Grepioni, E. Parisini, B.F.G. Johnson, C.M. Martin, J.G.M. Nairn, J. Lewis and M. Martinelli, *J. Chem. Soc., Dalton Trans.*, (1992) 15.
[4] D. Braga and F. Grepioni, *Acc. Chem. Res., 27* (1994) 51.
[5] See, for example, (a) V.W.W. Yam, W.K. Lee and T.F. Lai, *Organometallics, 12* (1993) 2383; (b) V.W.W. Yam, L.P. Chan and T.F. Lai, *Organometallics, 12* (1993) 2197; (c) V.W.W. Yam, W.K. Lee and T.F. Lai, *J. Chem. Soc., Chem. Commun.*, (1993) 1517; (d) V.W.W. Yam, L.P. Chan and T.F. Lai, *J. Chem. Soc., Dalton Trans.*, (1993) 2075; (e) V.W.W. Yam and W.K. Lee, *J. Chem. Soc., Dalton Trans.*, (1993) 2097; (f) V.W.W. Yam, K.K. Tam and T.F. Lai, *J. Chem. Soc., Dalton Trans.*, (1993) 651.
[6] R.J. Cross and M.F. Davidson, *J. Chem. Soc., Dalton Trans.*, (1986) 411.
[7] G.E. Coates and C. Parkin, *J. Chem. Soc.*, (1962) 3220.
[8] T.E. Müller, D.M.P. Mingos, D.J. Williams, *J. Chem. Soc., Chem. Commun.*, (1994), 1781.
[9] H.S. Rzepa, M.H. Smith, M.L. Webb, *J. Chem. Soc., Perkin Trans. 2*, (1994) *703*.
[10] A. Furlani, S. Licoccia, M.V. Russo, A.C. Villa and C. Guastini, *J. Chem. Soc., Dalton Trans.*, (1984) 2197.
[11] C.A. Tolman, *Chem. Rev., 77*, No. 3 (1977) 31.
[12] *CaChe, Release 3.5.1*, CAChe Scientific, Beaverton, 1993.
[13] See, for example, (a) C. Kutal, *Coord. Chem. Rev., 99* (1990) 213; (b) D.P. Segers, M.K. DeArmond, P.A. Grutsch and C. Kutal, *Inorg. Chem., 23* (1984) 2874; (c) P.A. Grutsch and C. Kutal, *J. Am. Chem. Soc., 101* (1979) 4228; (d) B. Liaw, S.W. Orchard and C. Kutal, *Inorg. Chem., 27* (1988) 1311; (e) M. Kasha and H.R. Rawls, *Photochem. Photobiol., 7* (1968) 561; (f) R.F. Ziolo, S. Lipton and Z. Dori, *J. Chem. Soc., Chem. Commun.*, (1970) 1124.
[14] A.J. Gordon, R.A. Ford, *The Chemist's Companion: a Handbook of Practical Data, Techniques and References*, Wiley-Interscience, New York, 1972.
[15] J. Wesemann, P.G. Jones, D. Schomburg, L. Heuer and R. Schmutzler, *Chem. Ber., 125* (1992) 2187.
[16] Y. Yang, V. Ramamoorthy and P.R. Sharp, *Inorg. Chem., 32* (1993) 1946.
[17] G.E. Coates and C. Parkin, *J. Chem. Soc.*, (1962) 3220.
[18] G.M. Sheldrick, *SHELXTL PC, Version 4.2*, Siemens Analytical X-ray Instruments, Madison, WI, 1990.
[19] B.J. Dunne, A.G. Orpen, *Acta Crystallogr., Sect. C, 47* (1991) 345.
[20] T.S. Cameron, K.D. Howlett and K. Miller, *Acta Crystallogr., Sect. B*, 34 (1978) 1639.
[21] J.A. Adeleke and L.K. Liu, *Acta Crystallogr., Sect. C, 49* (1993) 680.
[22] A. Houlton, R.M.G. Roberts, J. Silver and M.G.B. Drew, *J. Chem. Soc., Dalton Trans.*, (1990) 1543.